Registration of myocardial PET and SPECT for viability assessment using mutual information

Martina Marinelli[a)]
*Nuklearmedinische Klinik der TU München, Ismaningerstraße 22, 81675 München, Germany
and Scuola Superiore Sant'Anna, Piazza Martiri della Libertà, 33, 56127 Pisa, Italy*

Axel Martinez-Möller and Brian Jensen
*Nuklearmedinische Klinik der TU München, Ismaningerstraße 22, 81675 München, Germany
and Computer Aided Medical Procedures and Augmented Reality, Fakultät für Informatik/I16,
TU München, Boltzmannstraße 3, 85748 Garching bei München, Germany*

Vincenzo Positano
Fondazione G. Monasterio CNR–Regione Toscana, Via Moruzzi 1, 56124 Pisa, Italy

Susanne Weismüller
Nuklearmedinische Klinik der TU München, Ismaningerstraße 22, 81675 München, Germany

Nassir Navab
*Computer Aided Medical Procedures and Augmented Reality, Fakultät für Informatik/I16,
TU München, Boltzmannstraße 3, 85748 Garching bei München, Germany*

Luigi Landini
Department of Information Engineering, University of Pisa, Via Diotisalvi 2, 56126 Pisa, Italy

Markus Schwaiger and Stephan G. Nekolla
Nuklearmedinische Klinik der TU München, Ismaningerstraße 22, 81675 München, Germany

Purpose: The combination of sequentially acquired cardiac PET and SPECT data integrating metabolic and perfusion information allows the assessment of myocardial viability, a relevant clinical parameter for the management of patients who have suffered myocardial infarction and are now candidates for complex and cost intensive therapies such as bypass surgery. However, registration of cardiac functional datasets acquired on different imaging systems is limited by the difficulty to define anatomical landmarks and by the relatively poor inherent spatial resolution. In this article, the authors sought to evaluate whether it is possible to automatically register FDG-PET and sestamibi-SPECT cardiac data.

Methods: Automatic rigid registration was implemented with the ITK framework using Mattes mutual information as the similarity measure and a quaternion to represent the rotational component. The goodness of the alignment was evaluated by computing the mean target registration error (mTRE) at the myocardial wall. The registration parameters were optimized for robustness and speed using the data from 11 cardiac patients undergoing both PET and SPECT examinations (training datasets). The optimized algorithm was applied on the PET and SPECT data from 11 further patients (evaluation datasets). Quantitative (mTRE calculation) and visual (scoring method) comparisons were performed between automatic and manual registrations. Moreover, the automatic registration was also compared to the registration implicitly defined in the standard clinical analysis.

Results: The registration parameters were successfully optimized and resulted in a mean mTRE of 1.13 mm and 1.2 s average runtime on standard computer hardware for the training datasets. Automatic registration in the 11 validation datasets resulted in an average mTRE of 2.3 mm, with 7.5 mm mTRE in the worst case and an average runtime of 1.6 s. Automatic registration outperformed manual registrations both for the mTRE and for the visual assessment. Automatic registration also resulted in higher accuracy and better visual assessment as compared to the registration implicitly performed in the standard clinical analysis.

Conclusions: The results demonstrate the possibility to successfully perform mutual information based registration of PET and SPECT cardiac data, allowing an improved workflow for the sequentially acquired cardiac datasets, in general, and specifically for the assessment of myocardial viability. © *2010 American Association of Physicists in Medicine*. [DOI: 10.1118/1.3395554]

Key words: registration, mutual information, functional images, myocardial viability

I. INTRODUCTION

The assessment of myocardial viability allows the discrimination between reversible contractile dysfunction, as in stunned or hibernating myocardium, and scarred, nonviable myocardial tissue. This discrimination allows defining the risk to benefit ratio for revascularization surgery and identifying the best therapeutic approach for each patient.

The assessment of myocardial viability can be accurately performed by positron emission tomography (PET) using ^{18}F-fluorodeoxyglucose (FDG) and ^{13}N-ammonia for the metabolic and perfusion studies, respectively.[1–4] However, a ^{13}N-ammonia-PET examination requires having a cyclotron on-site because of its short physical half-life of 10 min. For this reason, an alternative protocol combining the metabolic information obtained by FDG-PET with a ^{99}Tc-sestamibi perfusion single-photon emission computed tomography (SPECT) examination is widely used.[5–10]

In this context, the volumetric datasets used for the viability study are acquired at two time points by different tomographs. Thus, retrospective, manual alignment is necessary for the viability assessment as for every region in the heart flow and metabolism information is compared. Typically, this comparison is performed at the image level with a "mental integration" by the clinical reader, thus introducing a substantial variability. This visual approach can be improved with volumetric data analysis, resulting in tracer uptake polar maps[22] and previously validated algorithms.[3] For this purpose, a visual matching of the polar maps generated by reorientation of the two volumetric datasets is clinically used. This approach implicitly assumes that both cardiac axes used for reorientation are defined exactly in the same way in both datasets. However, such an approach could be still error-prone because of the difficulty to define the same axes in two datasets showing different functional information as well as for the intra- and interobserver variability in the definition of the axes. This problem is further increased by large perfusion and metabolic defects (i.e., reduction in or absence of tracer uptake) typically seen in patients undergoing a viability examination due to the severity of myocardial disease. Therefore, we consider it advantageous to have an image registration algorithm integrated into the viability study providing coregistered volumetric datasets as input for the analysis.

Automatic registration of cardiac PET and SPECT data has been scarcely reported in literature. Gilardi *et al.*[11] proposed performing surface matching on the so-called transmission images. The transmission images contain morphological information rather than functional information, showing the radiodensity of each voxel which can be acquired to correct for the photon attenuation occurring during the acquisition. Also Eberl *et al.*[12] aligned transmission images from PET and SPECT using in this case a voxel based similarity metric. Although using the transmission data could be beneficial for the registration, this method is not widely applicable because transmission images are rarely acquired in SPECT[13,14] as special hardware (e.g., SPECT/CT systems) is needed and, when they are acquired, misregistration of the transmission and emission images is relatively frequent.[15,16]

Thus, an automated method aligning emission data would improve the diagnostic accuracy by reducing alignment errors.

The definition of anatomical landmarks in this context is challenging and prone to error due to the functional rather than morphological nature of the data, especially when a pathological defect in the myocardium is present. For this reason, the use of a voxel based similarity metric, such as mutual information,[17,18] could improve the registration of multimodal emission datasets. However, no previous work is available on using mutual information to register cardiac PET and SPECT data.

In this paper, we present an automatic registration algorithm based on the Mattes mutual information[19] and on a local optimization process to align PET and SPECT datasets, respectively, providing information on the myocardial metabolism and perfusion. The method was implemented by using the ITK framework[20,21] and integrating different open source components developed in C++. The clinical efficiency and accuracy of the implemented registration algorithm was severely affected by the values of several parameters involved in the process. The first purpose of the presented work was the optimization of these parameters to make the registration useful in a clinical setting. The robustness was set as the main priority in order to have the highest success rate possible and the execution time was defined as a secondary objective, with a runtime below 5 s being desirable to avoid interfering with the regular clinical workflow.

The registration method used is not pioneering since it is based on the previously published methods, but this work is unique in its application for the particular requirements of cardiac PET and SPECT emission data. Indeed, these data are similar with respect to motional blurring (respiratory motion and cardiac contraction) and relatively poor inherent spatial resolution, but show very different intensity patterns because of their functional nature (Fig. 1).

A preliminary version of the method was previously presented.[23] In this work, we improved the described approach in order to have higher success rate for the registration and to make it faster. For this purpose, 11 training datasets for the development of the method and 11 evaluation datasets for the assessment were used. Moreover, the reference alignment of each dataset was determined in order to calculate the accuracy of the approach. The best combination of five registration parameters, three for the optimizer, and two for the mutual information metric was selected by considering the success rate and the execution time.

The developed registration algorithm was evaluated by applying it to the evaluation datasets and comparing the calculated results to the manual registration performed by two experienced observers. Moreover, we evaluated the potential clinical application of the developed method by integrating it in a previously validated software for analysis of nuclear cardiac examinations.
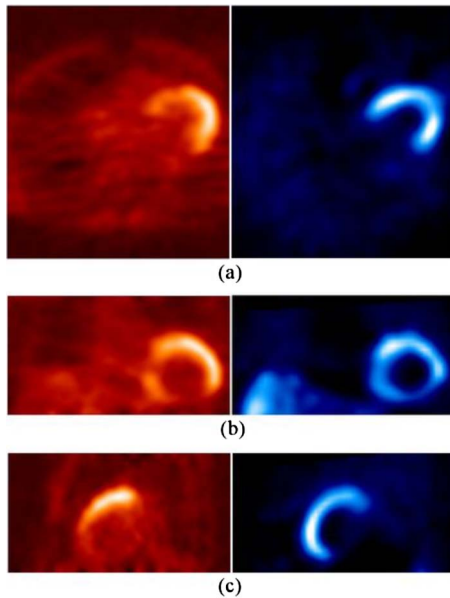
FIG. 1. Transaxial (a), coronal (b), and sagittal (c) corresponding views of ^{18}F-FDG PET (left column) and [99 m]Tc-sestamibi SPECT (right column) examinations of the same patient for the assessment of myocardial viability showing high left ventricular uptake in both cases. Notable differences in signal distribution are visible.

II. MATERIALS AND METHODS

II.A. Patient population

Twenty-two consecutive patients, who underwent a sequentially acquired PET and SPECT protocol for assessment of myocardial viability, were included in this study (age: 71 ± 8 yr, 18 males and 4 females). From the 22 patients, only one was classified as normal, that is, without perfusion or metabolic deficit. A mismatch area indicating viable tissue was present in $n=18$ patients (average extent of left ventricle: $25 \pm 16\%$ LV) and a scar area indicating nonviable tissue was present in $n=16$ patients (average extent: $30 \pm 15\%$ LV).

II.B. Data acquisition and reconstruction

The PET acquisition was performed using a Siemens ECAT HR+ starting 30–60 min after injection of ^{18}F-FDG. Images were reconstructed using filtered backprojection with a Hanning filter (cut-off frequency: 0.2 cycles/pixel), resulting in a volume of $128 \times 128 \times 63$ voxels, with a voxel size of $2.3 \times 2.3 \times 3.9$ mm^3. Attenuation correction was performed by means of a rotating [68]Ge rod source. The reported transaxial spatial resolution of the PET system in two-dimensional mode is 4.3 mm at the center of the field of view and increases to 4.7 mm tangential and 8.3 mm radial at a distance of 20 cm from the center.[24]

The SPECT acquisition was performed using a dual-headed Siemens E.CAM equipped with low-energy high-resolution collimators starting 30–60 min after injection of [99 m]Tc-sestamibi. Images were reconstructed using filtered backprojection with a Butterworth filter (fifth order, cut-off frequency: 0.60 cycles/cm), resulting in a $64 \times 64 \times 32$ vol-
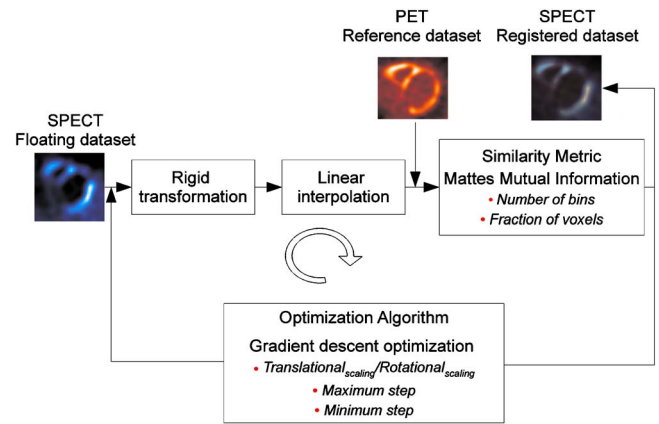

FIG. 2. Scheme of the developed registration algorithm. The five parameters affecting the success of the alignment process in clinical application are shown in the respective boxes.

ume with a voxel size of $6.6 \times 6.6 \times 6.6$ mm^3. Attenuation correction was not performed since it is not available on this scanner. The reported spatial resolution of the SPECT system is 9.1 mm.[25]

Representative views of the examinations are shown in Fig. 1. Both acquisitions were performed on the same day, with a typical delay of 1–3 h. It is important to note that the quoted spatial resolution values for both scanners were obtained in experimental phantom studies. The observed resolution in patient scans is worse, diminished by the cardiac and respiratory movements present during the acquisition.

Before the application of the registration algorithm, the PET and SPECT datasets were resampled using linear interpolation to produce two isotropic volumes with a slice matrix of 128×128 and a voxel size of $2.3 \times 2.3 \times 2.3$ mm^3. Eleven pairs of PET and SPECT datasets (training datasets) were randomly selected and used as base of knowledge to optimize the parameters of the automatic registration algorithm, while the other datasets (evaluation datasets) were used for the performance assessment of the developed method.

II.C. Registration algorithm

The registration algorithm was implemented in C++ using the Insight Toolkit (ITK) framework,[20] which provides a library of functions to perform different image processing operations and is particularly well suited as a starting point for the development of segmentation and registration applications.

The pipeline of our registration approach, shown in Fig. 2, was built by defining four main steps: the floating dataset geometrical transformation, the interpolation method, the evaluation of the similarity metric, and optimization procedure that estimates the optimal transformation to maximize the similarity. The process was iterated until a maximum of the similarity metric was reached.

It was decided to initialize the transformation by aligning the geometrical center of both images (using the class *itk-::CenteredTransformInitializer*) since the SPECT and PET data show very different intensity distributions. In particular, the liver often shows higher tracer uptake in the SPECT but only modest uptake in the FDG-PET data, as shown in Fig. 1.

We used a rigid transformation (*itk::VersorRigid3D-Transform*) as the basis of the algorithm. In this class, the translation is defined by a three-element vector and the rotation is represented as a versor or unit quaternion, described by three parameters. We decided to use this approach in order to overcome some of the limitations from the Euler angle representation, such as the gimbal lock[26,27] that occurs when the second Euler angle value is equal to 90°, leading to the loss of a degree of freedom.

The Mattes mutual information[19] was chosen as the similarity measure. Mutual information allows dealing with differences in the image intensities and is thereby well adapted for intermodality image registration. Moreover, the implementation proposed by Mattes *et al.* presents several advantages, which make the registration more robust to the effects caused by the quantization from interpolation and discretization from binning data, such as the use of a Parzen window to generate the joint histograms and the use of the same spatial sample set during the whole registration process, which smoothes the pattern for the metric value. For the Mattes mutual information metric, two parameters have influence on its efficiency: the number of bins (bins) used to calculate the joint histogram and the fraction of voxels (samples) sampled for the estimation of the metric.

Finally, a variant of the gradient descent optimization specific for versor space was used (*itk::VersorRigid3D-TransformOptimizer*), and linear interpolation was performed for the transformed images. As shown in Fig. 2, three parameters affected the clinical efficiency of the used optimization algorithm: the ratio between the scaling factors in translational ($T_{scaling}$) and rotational ($R_{scaling}$) spaces that allow one to scale the steps given by the optimizer, the maximum step size (max step) used at the start of the optimization, and the minimum step size (min step) representing the convergence criterion of the optimization.

The five parameters (three for the optimization and two for the similarity measure) affecting the proposed registration algorithm were determined by evaluation with the training datasets, as described below. Although minimization of the execution time was not a primary objective of this work, the registration algorithm was implemented in order to work in several parallel processes so as to exploit the possibilities offered by multiprocessor computers. Moreover, for visualization purposes and also to allow performing manual registration, a graphical user interface was developed by using the Qt framework. The interface shows transverse, coronal, and sagittal fused views and allows switching to a checkerboard view.

In all cases described below, the registration process was applied by considering PET as the reference dataset and SPECT as the floating dataset. All automatic registrations were performed on a laptop equipped with an Intel Core 2 Duo T5500 processor working at 1.66 GHz.

II.D. Definition of the gold standard

In this work, the optimization and the evaluation of the automatic registration algorithm required a gold standard regarding the alignment and a technique to evaluate the goodness of the registration. As reported by Mäkelä *et al.*,[28] the definition of the gold standard bases mostly on the use of external fiducial markers or manually defined anatomical landmarks. For its application in patients, the use of fiducial markers on the heart had to be discarded. Moreover, the complementary functional information provided by PET and SPECT made the definition of the corresponding anatomical points challenging and error-prone, as well as making manual registration by an expert observer insufficient for the definition of a reference position. Therefore, a well-defined ground truth was not available. Consequently, a method described in literature to find a reference alignment[29,30] was used instead: the registration algorithm, with the parameters reported in Martinez-Möller *et al.*,[23] was applied 30 times on each pair of PET and SPECT datasets after randomly misaligning them by up to ±30 mm for each translational parameter and ±10° for each rotational parameter. Subsequently, an expert observer assessed the quality of all 30 registrations, classifying them as positive (perfectly aligned) or negative (errors in the alignment). The gold standard was defined as being the average transformation of all registrations evaluated positively by the observer.

II.E. Method to quantitatively evaluate the goodness of a registration result

The result of a registration was evaluated by comparison with the defined gold standard. The goodness of a registration result was evaluated only at the left ventricle. In order to define the points where the accuracy is to be evaluated, the cardiac axis of the floating dataset was manually defined by an experienced operator and used to sample the myocardial wall in 460 points, according to the method reported in Nekolla *et al.*[22] This approach is frequently performed in order to extract a polar map summarizing the information contained in the three-dimensional tomographic data.[31] The mean target registration error (mTRE) was computed as the average over the 460 sampling points of the Euclidean distance between the spatial coordinates in the transformation to be evaluated and the corresponding points in the gold standard transformation.

Additionally, we sought to estimate the maximum alignment error tolerated by the observer with the PET and SPECT data in order to classify a registration result as successful. For this purpose, for each training dataset we computed the maximum mTRE of all registrations which had been previously evaluated positively (see Sec. II D). The tolerance bandwidth was defined as the 75th percentile of the maximum mTREs on all training datasets.

TABLE I. Search space for the registration parameters.

	Range
$T_{\text{scaling}}/R_{\text{scaling}}$	3×10^{-3}, 3×10^{-4}, 3×10^{-5}, 3×10^{-6}
Maximum step size (mm)	2.3, 3.3
Minimum step size (mm)	0.1, 0.2, 0.3
No. of bins	30, 35, 40, 45, 50, 55, 60, 65, 70
Sample size	0.01, 0.05, 0.1, 0.2, 0.3, 0.4, 0.5

II.F. Optimization of the registration parameters

The clinical success and performance of a registration process heavily depends on using parameters well adapted to the data to be registered. As described above, we sought to find values for five different parameters used in our algorithm in order to achieve a good compromise between robustness and execution time. We investigated three parameters used in the optimization: the ratio between translational (T_{scaling}) and rotational scaling (R_{scaling}) (modifying the translational scaling T_{scaling} by setting the rotational scaling R_{scaling} to a constant value of 1), the maximum step size (max step) and the minimum step size (min step), and two more parameters used to compute the Mattes mutual information metric, the number of bins (bins), and the fraction of voxels (samples).

The search space for the parameters was limited to a reduced range of values (Table I) in order to be able to execute the algorithm for all training datasets within a reasonable amount of time. The selection of the range of values was done by adapting values suggested in Ibanez *et al.*[20] for the spatial resolution and physical size of the PET and SPECT data to be registered.

For each combination of parameters, the registration of all PET and SPECT training datasets was performed automatically, saving the resulting transformation parameters, the computational time as well as the computed mTRE. A registration was considered successful if the mTRE was within the previously defined bandwidth (see Sec. II E). Since several combinations of parameters resulted in a 100% success rate, the combination resulting in the best compromise between mTRE and runtime was chosen.

II.G. Evaluation of the automatic registration algorithm

The registration algorithm with the combination of parameters found in Sec. II F was applied to the PET and SPECT evaluation datasets and the mTREs were calculated. A registration was considered successful if the mTRE was within the tolerance bandwidth.

II.H. Comparison with manual registration

We sought also to compare the automatic method with the manual registration performed by two expert observers (A and B). The manual registration aimed at achieving a high visual accuracy at the expense of a long processing time. The observers adjusted all six transformation parameters while evaluating the fused views and occasionally switching the views to a checkerboard display using the graphical user interface (see Sec. II C). The mTRE values were also computed for the manual registrations.

In addition to the mTRE, the automatic and manual registrations of the evaluation datasets classified as successful by the automatic alignment (see Sec. II G) were visually evaluated by the two observers A and B, blinded to the registration approach used. For each evaluation dataset, the three pairs of registered images (automatic, manual-A, and manual-B) were shown besides each other in a random order. The two observers gave a score to each registration, depending on the visual goodness of the spatial alignment. A three point scale was used: The score 1 was given to datasets which showed a small bias in the matching; the score 2 was given to datasets which appeared to be "well aligned;" and the score 3 was given to "perfectly aligned" datasets.

II.I. Comparison of the registration algorithm to the standard clinical workflow

In the standard clinical workflow, the registration is implicitly achieved by manually defining the cardiac axis on PET and SPECT images separately. For each evaluation dataset, two expert observers (A and B) performed the standard analysis using the validated software for the analysis of nuclear cardiac examinations.[3,22] The implicit spatial transformation was determined in terms of unit quaternion and translation vector using the Horn method,[26] which presents a closed-form solution to the least-squares problem of rigidly matching different sets of coordinates (the myocardial sampling points resulting from the manual cardiac axis definition were used for this purpose). This method is summarized in Fig. 3(a). The manually defined PET cardiac axis and the report page showing the reoriented cardiac views (called in the text "manual report page") of both PET and SPECT studies were saved for each observer. Moreover, to quantitatively evaluate the goodness of the registration result, the determined Horn transformation was applied to the myocardial points defined in Sec. II D and the mTRE was calculated.

The automatic registration algorithm was integrated into the analysis software and used to register the PET and SPECT evaluation datasets. The previously saved PET cardiac axis was then applied to the registered SPECT dataset [Fig. 3(b)], and a report page (called in the text "automatic report page") was created.

The automatic and manual report pages of the evaluation datasets classified as successful by the automatic alignment (see Sec. II G) were visually compared by two observers A and B, blinded to the registration method. For each evaluation dataset, the four report pages (automatic-A, automatic-B, manual-A, and manual-B) were shown. The two observers gave a score to each report page, depending on the visual evaluation of the spatial alignment using the three point scale described in Sec. II H.
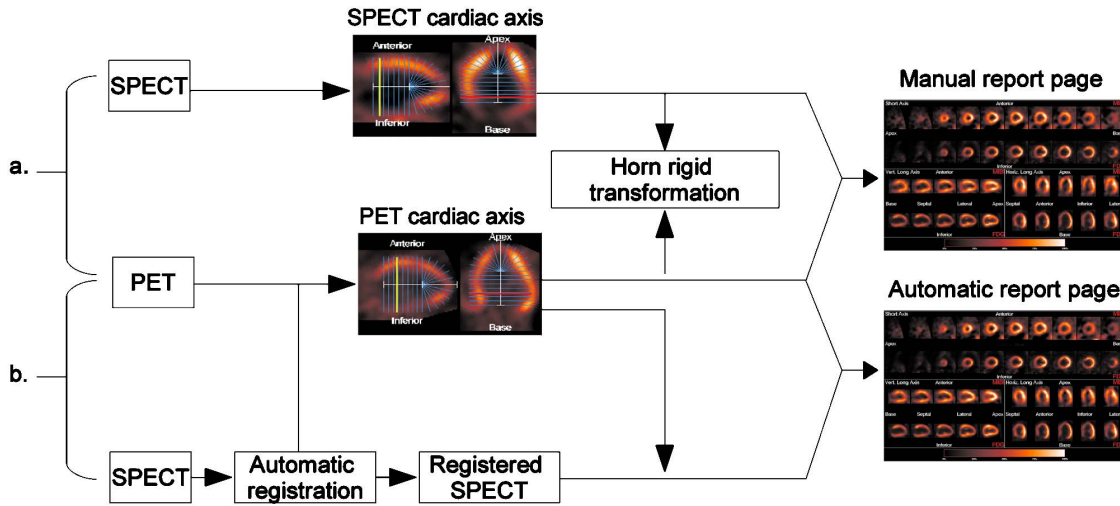
FIG. 3. Method used to compare the automatic registration result to the registration implicitly defined in the standard clinical analysis. Diagram (a) shows the creation of the manual report page using the manual definition of the cardiac axis on both datasets. Diagram (b) shows the creation of the automatic report page using the manual definition of the PET cardiac axis and its application to the automatically registered SPECT dataset.

III. RESULTS

III.A. Optimization of the registration parameters

The tolerance bandwidth for the mTRE was found to be 3.27 mm, computed according to Sec. II D. Table II shows the registration parameters and the average mTRE for the first ten combinations of parameters for all 11 training datasets. Using these results, the best combination of parameters was determined to be $T_{scaling}=3\times10^{-5}$, $R_{scaling}=1$, maximum step=3.3 mm, minimum step=0.3 mm, number of bins=55, and sample size=0.05 (highlighted in Table II). This combination resulted in an average mTRE of 1.13 mm and a mean runtime of 1.2 s.

III.B. Evaluation of the automatic registration algorithm

The registration algorithm with the combination of parameters described above was then applied to the evaluation datasets. A representative example of PET and SPECT datasets before and after the application of the automatic registration is shown in Fig. 4. The results of the registration are summarized in the second column (reference vs automatic) of Table III, showing the mTRE for each evaluation dataset.

According to the tolerance bandwidth, the automatic registration was successful in 10/11 cases (91%). For the successful registration cases, the average mTRE was 1.9 mm. In the dataset which was considered unsuccessful (Fig. 5), the mTRE was 7.5 mm. The average mTRE for both successful and unsuccessful registrations together was 2.3 mm.

III.C. Comparison with manual registration

The results of the manual alignment together with the corresponding interobserver difference, defined as the Euclidean distance in the target region between the manual registrations by observers A and B, are shown in Table III.

For the manual registration, an average mTRE of 2.7 mm was found for observer A and 5.4 mm for observer B. Application of the same tolerance bandwidth for the manual registration results in successful registration in 9/11 cases (82%)

TABLE II. Mean target registration error and execution time in the training datasets for the first ten combinations of parameters ordered by considering the average mTRE. For all combinations $T_{scaling}=3\times10^{-5}$ and $R_{scaling}=1$. The mTREs are reported in mm and the execution times in seconds.

Combination parameters					
Sample size	Bin	Max step	Min step	Average mTRE	Time
0.2	70	3.3	0.3	1.06	5.03
0.3	70	2.3	0.3	1.08	7.97
0.4	70	2.3	0.3	1.10	10.19
0.2	65	2.3	0.3	1.12	5.55
0.05	**55**	**3.3**	**0.3**	**1.13**	**1.20**
0.3	60	2.3	0.3	1.14	8.04
0.05	55	2.3	0.3	1.14	1.48
0.1	70	2.3	0.2	1.15	3.44

TABLE III. Mean target registration error (mm) for each evaluation dataset resulting from the automatic and manual registrations. The interobserver difference is also shown.

	Reference vs automatic	Reference vs manual-A	Reference vs manual-B	Manual-A vs manual-B
1	7.52	2.42	5.79	4.72
2	0.63	1.08	3.05	3.51
3	1.00	2.09	8.96	8.35
4	3.18	3.71	7.44	9.80
5	1.54	1.82	3.07	3.72
6	1.04	6.78	3.26	5.35
7	2.38	1.53	8.04	7.30
8	2.88	1.70	3.86	2.60
9	2.69	2.83	6.68	6.71
10	1.90	3.06	2.35	2.30
11	1.00	2.62	6.45	4.23
Average mTRE	2.34	2.69	5.36	5.33[a]
Success rate	10/11	9/11	4/11	–

[a]Average distance at target points between the registrations of both observers.

for observer A and 4/11 cases (36%) for observer B. The average interobserver difference was 5.3 mm.

The scores of the visual evaluation of the registration are shown in Table IV. According to the score assigned in average by both observers A and B, the automatic registration obtained the best average score. For both observers, the score assigned to the automatic registration was higher than the score assigned to the other observer. The mean processing time was 1.6 s for each automatic registration and about 15 min for each manual registration.
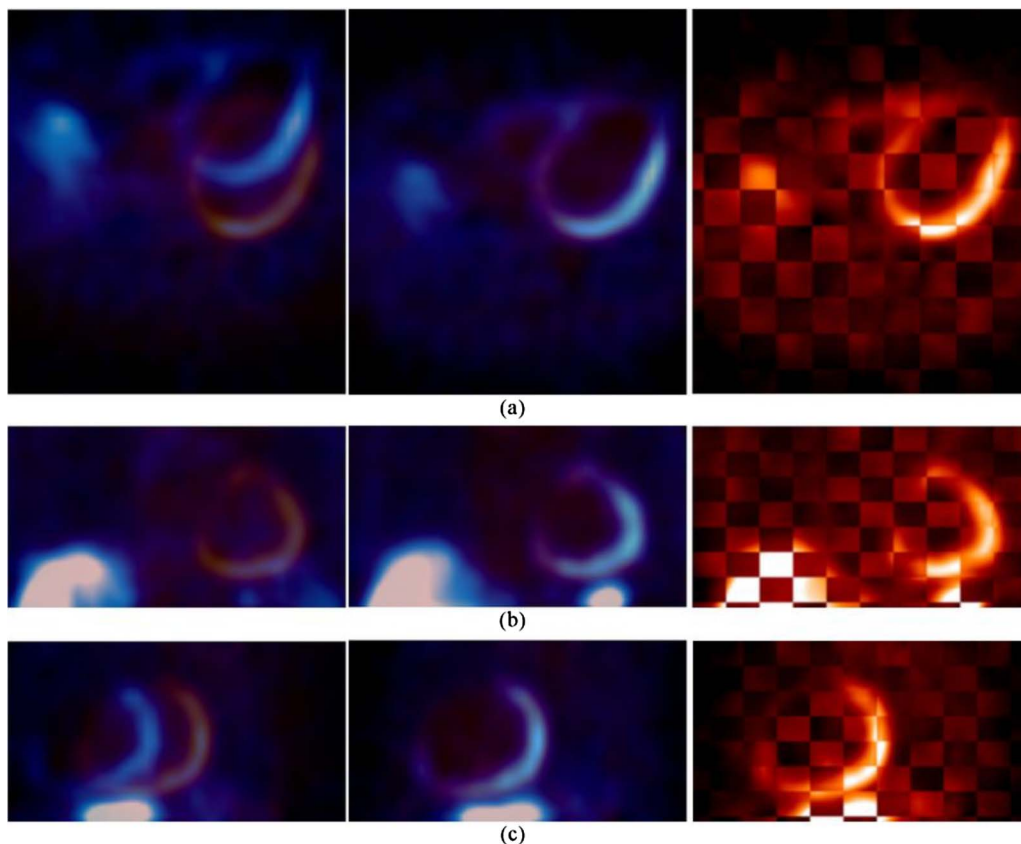

FIG. 4. Transaxial (a), coronal (b), and sagittal (c) cardiac views of the FDG-PET and the sestamibi-SPECT datasets before (left column) and after (middle and right columns) the automatic registration. In the right column, a checkerboard display is shown. A correct alignment of the two datasets is obtained.

TABLE IV. Score assigned by the two observers A and B to the automatic, manual-A, and manual-B successful registrations. An average score value (A and B) is shown in the top row.

Evaluation	Registration		
	Automatic	Manual-A	Manual-B
A and B	2.1	2.0	2.0
A	2.4	2.4	2.1
B	1.8	1.6	1.8

TABLE VI. Score assigned by the two observers A and B to the registration in the automatic-A, automatic-B, manual-A, and manual-B report pages. An average score value (A and B) is shown in the top row.

Evaluation	Registration			
	Automatic-A	Manual-A	Automatic-B	Manual-B
A and B	2.3	1.8	2.6	2.1
A	2.7	1.8	2.8	2.0
B	1.9	1.9	2.3	2.2

III.D. Comparison of the registration algorithm to the standard clinical workflow

Using the standard clinical workflow, an average mTRE of 5.1 mm was found for observer A and 6.0 mm for observer B. Application of the same tolerance bandwidth for the manual registration results in successful registration in 3/11 cases (27%) for observer A and 2/11 cases (18%) for observer B (Table V).

The scores of the visual evaluation of the registration in the automatic and manual report pages are shown in Table VI. According to the score assigned in average by both observers A and B, the automatic registration obtained the best score. For observer A, the automatic method outperformed in all cases the manual method, while for observer B, no relevant difference was noticed between both. An example of manual and automatic report pages with selected short axis and horizontal and vertical long axes is shown in Fig. 6. Compared to the mean processing time of 1.6 s for each automatic registration, the standard clinical workflow needed about 1 min for the definition of the both cardiac axes.

IV. DISCUSSION

The registration of PET and SPECT cardiac datasets is important for the precise regional correlation between metabolic and perfusion information as needed for the assessment of myocardial viability. In the standard clinical workflow, the registration is implicitly achieved by manually defining the cardiac axis on PET and SPECT images separately. This leads to a time consuming and operator dependent process. Such process can be improved in perfusion SPECT imaging by automatic segmentation of the left ventricle.[32–34] However, there is no tool available to automatically perform this step in combined PET-SPECT viability studies so that manual definition of the cardiac axis is performed routinely for viability assessment. Moreover, automatic segmentation of the left ventricle has a limited success rate,[35] which might be lower in patients undergoing a viability study, often presenting large defects.

In this paper, we showed that PET and SPECT cardiac datasets can be automatically aligned using mutual information and that the developed registration method can be integrated within the regular clinical workflow. No similar approaches matching multimodality nuclear cardiac data have been previously reported in literature. Instead, other studies have proposed using the morphological information contained in the transmission images, approach which limits substantially its applicability.

In our work, rigid registration was chosen for the alignment because it is clinically required to preserve the geometry and the shape of the left ventricle in the data, which

TABLE V. Mean target registration error (mm) for each evaluation dataset resulting from the automatic alignment and from the registration implicitly performed in the standard clinical analysis. The interobserver difference is also shown.

	Reference vs automatic	Reference vs manual-A	Reference vs manual-B	Manual-A vs manual-B
1	7.52	5.29	10.19	6.31
2	0.63	3.14	1.65	3.39
3	1.00	7.50	3.87	9.39
4	3.18	3.04	3.31	5.36
5	1.54	3.32	2.56	2.45
6	1.04	6.63	5.83	3.91
7	2.38	8.50	8.77	5.53
8	2.88	3.00	8.74	6.83
9	2.69	3.84	6.93	4.83
10	1.90	6.22	7.58	3.85
11	1.00	6.14	6.13	7.01
Average mTRE	2.34	5.15	5.96	5.26[a]
Success rate	10/11	3/11	2/11	–

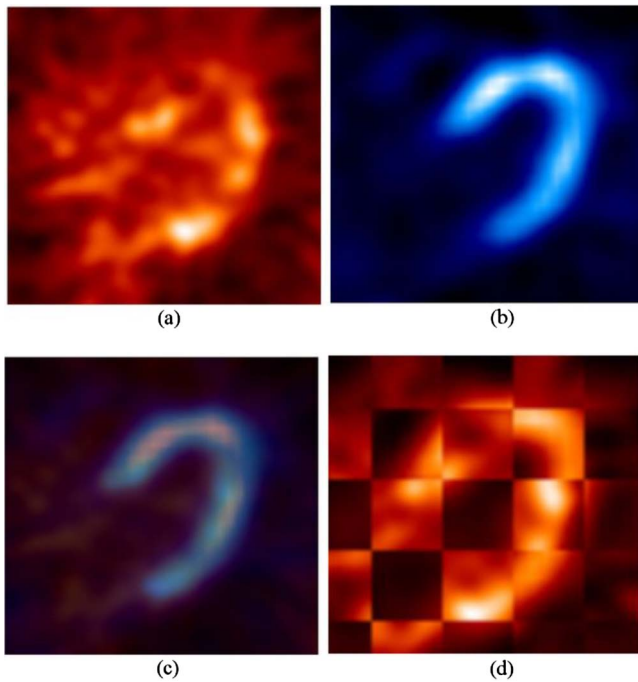[a]Average distance at target points between the registrations of both observers.

FIG. 5. Transaxial view of the left ventricle in the reference (a) and floating (b) datasets corresponding to the registration considered unsuccessful. The result of the automatic registration is shown at the bottom row as a fused image (c) and checkerboard display (d).
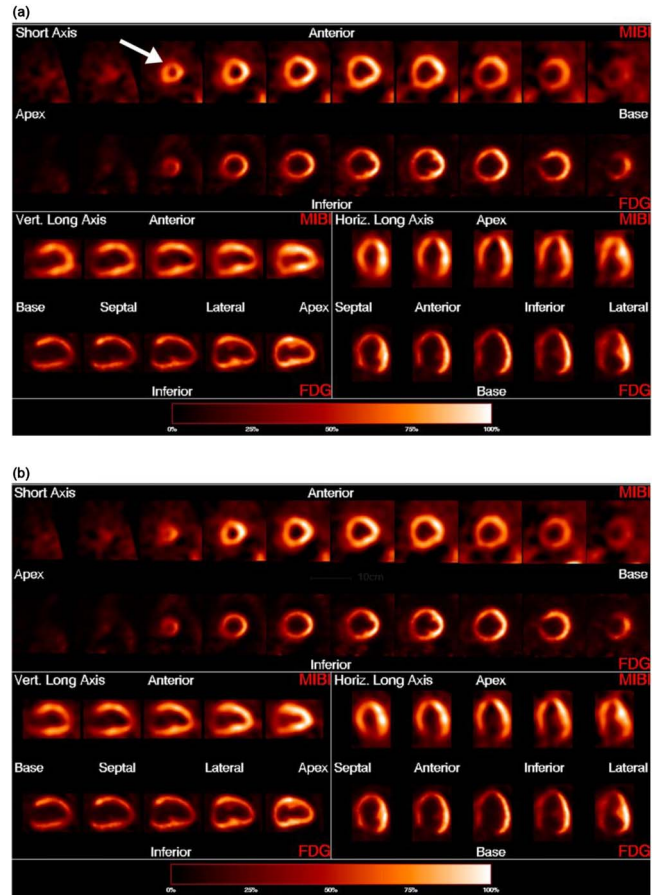

FIG. 6. Example of manual (a) and automatic (b) report pages for a combined PET/SPECT examination generated by observer A. As can be seen, the PET dataset was used as a reference image and thus remains unchanged between both report pages, whereas the SPECT dataset shows differences according to the registration approach. A registration bias in the manual report page is visible, as shown, for example, by the white arrow. Note especially the removal of the tilt of the cardiac studies along the long axis. For the manual report page, the calculated mTRE is 3.32. For the automatic report page, the mTRE is 1.54. Both observers gave a score=3 to the automatic report page. The manual report page obtained score=2 and score=1 by observers A and B, respectively.

provides additional information about the pathological condition. However, it could be interesting to extend the work investigating the effect of affine or spline based nonrigid registrations, which could eventually capture more detailed deformation and help overcome apparent alterations in the shape of the heart which might appear due to the nonisotropic image resolution.

An important limitation of this work is that, since it was performed on clinical patient images, the ground truth was not known, making it challenging to assess the accuracy of the registration. As alternative, we used a method reported to overcome this issue and find a reference alignment,[29,30] which was then used to optimize the registration parameters based on the mTRE on the training datasets. Also for the assessment of the myocardial viability no further gold standard was available, nor was a clinical end-point indicating the success rate of the eventually performed revascularization. Therefore, it was impossible to evaluate the eventual impact of the automatic registration on the diagnosis and clinical decision.

One result which is to be noted with some concern is that both the mTRE and the execution time for the training datasets are lower than for the evaluation datasets. This might reflect a lack of generality of the method which could be overcome by a larger number of datasets. Still, the global accuracy found for the automatic registration for both the training and validation datasets was very high. The average mTRE for the validation datasets, even when considering the patient above the tolerance bandwidth, is 2.3 mm, far below the nominal spatial resolution of SPECT data and thus well

suited for clinical routine use. Moreover, the case where the alignment was considered to fail (Fig. 5) shows an exceptionally low image quality for the PET data, pointing to a possible problem during the acquisition and, consequently, affecting the automatic registration process. This patient resulted in an mTRE of 7.5 mm, which is clearly noticeable, but it is to be put in perspective with the error performed by manual registration, which frequently results in higher inaccuracies (Table III).

By comparing mTRE values, automatic registration outperformed manual registration as well as the registration obtained by standard clinical analysis. Automatic registration also resulted in a higher success rate according to the tolerance bandwidth. Moreover, a very high interobserver variability was obtained, occasionally higher than the mTRE itself, supporting the fact that the alignment process needs to be made automatic to avoid a strong dependence on the operator.

As described in Fig. 3(b), integration of the algorithm within the clinical workflow allows one to define the cardiac axis only once and to apply it to both datasets. This approach can reduce the observer variability and also the time in the cardiac axis definition. Indeed, the operator can choose the dataset to use to define the cardiac axis, improving the confidence when large defects are present in the myocardium.

Automatic registration also resulted in a significant gain of analysis time, with automatic registration needing 1.6 s to execute, whereas manual registration targeting high accuracy required 15 min in average. Still, the speed of the algorithm was not a main priority for this work, and further improvements can be achieved with a refined implementation and approaches such as multiresolution.[18,29,30]

The automatic registration was also compared to the manual registration by a visual evaluation blinded to the way the registration was performed. The average score assigned to the automatic registration was higher than the score for the manual registration of either observer. It is interesting to note that a comparable score was given by each observer to the automatic method and to the registration performed by himself, while a worse score was assigned to the other observer. That is, the automatic registration appeared to satisfy both experts, but the manual registration by other experts was less satisfactory.

A visual comparison of manual and automatic report pages was also performed. The average visual score as evaluated by observer A was higher for the registration in the automatic report pages than for the registration in the manual report pages, while being nearly equivalent in the evaluation by observer B.

V. CONCLUSION

Registration of cardiac PET and SPECT data for assessment of myocardial viability was shown to be feasible using mutual information as the similarity measure and adapted optimization parameters. The integration of the method in the clinical workflow allows not only to decrease the processing time but also to eliminate interobserver variability and to reach registration results, which are superior to those achieved by manual registration.

ACKNOWLEDGMENT

a)Author to whom correspondence should be addressed. Electronic mail: m.marinelli@sssup.it; Telephone: +498941402968; Fax: +498941404841.

[1]V. Rizzello, D. Poldermans, and J. J. Bax, "Assessment of myocardial viability in chronic ischemic heart disease: Current status," Q. J. Nucl. Med. Mol. Imaging **49**, 81–89 (2005).

[2]M. D. Cerqueira and A. F. Jacobson, "Assessment of myocardial viability with SPECT and PET imaging," AJR, Am. J. Roentgenol. **153**(3), 477–483 (1989).

[3]F. Haas, C. J. Haehnel, W. Picker, S. Nekolla, S. Martinoff, H. Meisner, and M. Schwaiger, "Preoperative positron emission tomographic viability assessment and perioperative and postoperative risk in patients with advanced ischemic heart disease," J. Am. Coll. Cardiol. **30**(7), 1693–1700 (1997).

[4]R. S. Beanlands, G. Nichol, E. Huszti, D. Humen, N. Racine, M. Freeman, K. Y. Gulenchyn, L. Garrard, R. deKemp, A. Guo, T. D. Ruddy, F. Benard, A. Lamy, and R. M. Iwanochko, "F-18-fluorodeoxyglucose positron emission tomography imaging-assisted management of patients with severe left ventricular dysfunction and suspected coronary disease: A randomized, controlled trial (PARR-2)," J. Am. Coll. Cardiol. **50**(20), 2002–2012 (2007).

[5]X. Zhang, X. Liu, S. Hu, T. H. Schindler, Y. Tian, Z. He, R. Gao, Q. Wu, H. Wei, J. W. Sayre, and H. R. Schelbert, "Long-term survival of patients with viable and nonviable aneurysm assessed by $^{99\,m}$Tc-MIBI SPECT and ^{18}F-FDG PET: A comparative study of medical and surgical treatment," J. Nucl. Med. **49**, 1288–1298 (2008).

[6]J. vom Dahl, C. Altehoefer, F. H. Sheehan, P. Buechin, R. Uebis, B. J. Messmer, U. Buell, and P. Hanrath, "Recovery of regional left ventricular dysfunction after coronary revascularization: Impact of myocardial viability assessed by nuclear imaging and vessel patency at follow-up angiography," J. Am. Coll. Cardiol. **28**, 948–958 (1996).

[7]J. vom Dahl, C. Altehoefer, F. H. Sheehan, P. Buechin, G. Schulz, E. Ruediger Schwarz, K. C. Koch, R. Uebis, B. J. Messmer, U. Buell, and P. Hanrath, "Effect of myocardial viability assessed by technetium-99m-sestamibi SPECT and fluorine-18-FDG PET on clinical outcome in coronary artery disease," J. Nucl. Med. **38**, 742–748 (1997).

[8]M. J. Knuuti, M. Saraste, P. Nuutila, R. Härkönen, U. Wegelius, A. Haapanen, J. Bergman, M. Haaparanta, T. Savunen, and L. M. Voipio-Pulkki, "Myocardial viability: Fluorine-18-deoxyglucose positron emission tomography in prediction of wall motion recovery after revascularization," Am. Heart J. **127**, 785–796 (1994).

[9]J. J. Bax, J. H. Cornel, F. C. Visser, P. M. Fioretti, A. van Lingen, A. E. M. Reijs, E. Boersma, G. J. J. Teule, and C. A. Visser, "Prediction of recovery of myocardial dysfunction after revascularization comparison of fluorine-18 fluorodeoxyglucose/thallium-201 SPECT, thallium-201 stress-reinjection SPECT and dobutamine echocardiography," J. Am. Coll. Cardiol. **28**, 558–564 (1996).

[10]G. Lucignani, G. Paolini, C. Landoni, M. Zuccari, G. Paganelli, L. Galli, G. Di Credico, G. Vanoli, C. Rossetti, M. A. Mariani, M. C. Gilardi, F. Colombo, A. Grossi, and F. Fazio, "Presurgical identification of hibernating myocardium by combined use of technetium-99m hexakis 2-methoxyisobutylisonitrile single photon emission tomography and fluorine-18 fluoro-2-deoxy-d-glucose positron emission tomography in patients with coronary artery disease," Eur. J. Nucl. Med. Mol. Imaging **19**, 874–881 (1992).

[11]M. C. Gilardi, G. Rizzo, A. Savi, C. Landoni, V. Bettinardi, C. Rossetti, G. Striano, and F. Fazio, "Correlation of SPECT and PET cardiac images by a surface matching registration technique," Comput. Med. Imaging Graph. **22**, 391–398 (1998).

[12]S. Eberl, I. Kanno, R. R. Fulton, A. Ryan, B. F. Hutton, and M. J. Fulham, "Automated interstudy image registration technique for SPECT and PET," J. Nucl. Med. **37**(1), 137–145 (1996).

[13]R. C. Hendel, "Attenuation correction: Eternal dilemma or real improvement?," Q. J. Nucl. Med. Mol. Imaging **49**, 30–42 (2005).

[14]G. Germano, P. J. Slomka, and D. S. Berman, "Attenuation correction in cardiac SPECT: The boy who cried wolf?," J. Nucl. Cardiol. **14**, 25–35 (2007).

[15]I. Matsunari, G. Boning, S. I. Ziegler, I. Kosa, S. G. Nekolla, E. P. Ficaro, and M. Schwaiger, "Effects of misalignment between transmission and emission scans on attenuation-corrected cardiac SPECT," J. Nucl. Med. **39**, 411–416 (1998).

[16]A. Martinez-Möller, M. Souvatzoglou, N. Navab, M. Schwaiger, and S. G. Nekolla, "Artifacts from misaligned CT in cardiac perfusion PET/CT studies: Frequency, effects, and potential solutions," J. Nucl. Med. **48**, 188–193 (2007).

[17]F. Maes, A. Collignon, D. Vandermeulen, G. Marchal, and P. Suetens, "Multimodality image registration by maximization of mutual information," IEEE Trans. Med. Imaging **16**(2), 187–198 (1997).

[18]W. M. Wells, P. Viola, H. Atsumi, S. Nakajima, and R. Kikinis, "Multimodal volume registration by maximization of mutual information," Med. Image Anal. **1**(1), 35–51 (1996).

[19]D. Mattes, D. R. Haynor, H. Vesselle, T. K. Lewellen, and W. Eubank, "PET-CT image registration in the chest using free-form deformations," IEEE Trans. Med. Imaging **22**(1), 120–128 (2003).

[20]L. Ibanez, W. Schroeder, L. Ng, J. Cates, and The Insight Software Consortium, The ITK Software Guide, 2nd ed., updated for ITK version 2.4, November 2005, available at http://www.itk.org/ItkSoftwareGuide.pdf.

[21]I. Wolf, M. Vetter, I. Wegner, T. Böttger, M. Nolde, M. Schöbinger, M. Hastenteufel, T. Kunert, and H. P. Meinzer, "The medical imaging interaction toolkit," Med. Image Anal. **9**, 594–604 (2005).

[22]S. G. Nekolla, C. Miethaner, N. Nguyen, S. I. Ziegler, and M. Schwaiger, "Reproducibility of polar map generation and assessment of defect severity and extent assessment in myocardial perfusion imaging using positron emission tomography," Eur. J. Nucl. Med. Mol. Imaging **25**, 1313–1321 (1998).

[23]A. Martinez-Möller, B. Jensen, N. Navab, M. Schwaiger, and S. G. Nekolla, "Automatic cardiac PET-SPECT and SPECT-SPECT registration," J. Nucl. Med. **49**(S1), 31 (2008).

[24]G. Brix, J. Zaers, L. E. Adam, M. E. Bellemann, H. Ostertag, H. Trojan, U. Haberkon, J. Doll, F. Oberdorfer, and W. J. Lorenz, "Performance evaluation of a whole-body PET scanner using the NEMA protocol. National Electrical Manufacturers Association," J. Nucl. Med. **38**, 1614–1623 (1997).

[25]J. T. Kuikka, J. Yang, and H. Kiiliäinen, "Physical performance of the Siemens E.CAM gamma camera," Nucl. Med. Commun. **19**(5), 457–462 (1998).

[26]B. K. P. Horn, "Closed-form solution of absolute orientation using unit quaternions," J. Opt. Soc. Am. A **4**, 629–942 (1987).

[27]J. G. Parker, B. A. Mair, and D. R. Gilland, "Respiratory motion correction in gated cardiac SPECT using quaternion-based, rigid-body registration," Med. Phys. **36**(10), 4742–4754 (2009).

[28]T. Mäkelä, P. Clarysse, O. Sipilä, N. Pauna, Q. C. Pham, T. Katila, and I. E. Magnin, "A review of cardiac image registration methods," IEEE Trans. Med. Imaging **21**(9), 1011–1021 (2002).

[29]L. Tang, G. Hamarneh, and A. Celler, "Validation of mutual information-based registration of CT and bone SPECT images in dual-isotope studies," Comput. Methods Programs Biomed. **92**, 173–185 (2008).

[30]P. J. Slomka, D. Dey, C. Przetak, U. E. Aladl, and R. P. Baum, "Automated 3-dimensional registration of stand-alone ^{18}F-FDG whole-body PET with CT," J. Nucl. Med. **44**(7), 1156–1167 (2003).

[31]M. D. Cerqueira *et al.*, "Standardized myocardial segmentation and nomenclature for tomographic imaging of the heart: A statement for healthcare professionals from the Cardiac Imaging Committee of the Council on Clinical Cardiology of the American Heart Association," Circulation **105**, 539–542 (2002).

[32]J. C. Cauvin, J. Y. Boire, J. C. Maublant, J. M. Bonny, M. Zanca, and A. Veyre, "Automatic detection of the left ventricular myocardium long axis and center in thallium-201 single photon emission computed tomography," Eur. J. Nucl. Med. **19**, 1032–1037 (1992).

[33]G. Germano, P. B. Kavanagh, H. Su, M. Mazzanti, H. Kiat, R. Hachamovitch, K. F. Van Train, J. S. Areeda, and D. S. Berman, "Automatic reorientation of three-dimensional, transaxial myocardial perfusion SPECT images," J. Nucl. Med. **36**(6), 1107–1114 (1995).

[34]P. J. Slomka, G. A. Hurwitz, J. Stephenson, and T. Cradduck, "Automated alignment and sizing of myocardial stress and rest scans to three-dimensional normal templates using an image registration algorithm," J. Nucl. Med. **36**, 1115–1122 (1995).

[35]Y. Xu, P. Kavanagh, M. Fish, J. Gerlach, A. Ramesh, M. Lemley, S. Hayes, D. S. Berman, G. Germano, and P. J. Slomka, "Automated quality control for segmentation of myocardial perfusion SPECT," J. Nucl. Med. **50**, 1418–1426 (2009).